Comparative *ab initio* study of half-Heusler compounds for optoelectronic applications

Thomas Gruhn*
Institut für Anorganische Chemie und Analytische Chemie, Johannes Gutenberg Universität, Staudinger Weg 9, 55099 Mainz, Germany
(Received 17 June 2010; revised manuscript received 7 September 2010; published 30 September 2010)

For the advancement of optoelectronic applications, such as thin-film solar cells or laser diodes, there is a strong demand for new semiconductor materials with tailored structural and electronic properties. The eight-electron half-Heusler compounds include many promising materials with a big variety of lattice constants and band gaps. So far only a small number of them have been investigated. With the help of *ab initio* calculations, we have studied all possible configurations of ternary 1:1:1 compounds in the half-Heusler structure. We have investigated 648 half-Heusler materials, including compounds of the types I-I-VI, I-II-V, I-III-IV, II-II-IV, and II-III-III. For all compounds, we have optimized the lattice constant and determined the most stable arrangement of elements on the half-Heusler lattice sites. Preferred configurations and semiconductivities are compared for the different half-Heusler types. A discussion of the lattice geometries provides a parameter-free function for estimating the lattice constants. The calculated band gaps and lattice constants are used to select potential substitute materials for CdS in the buffer layer of $CuInSe_2$ and $Cu(In,Ga)Se_2$ thin-film solar cells.

DOI: 10.1103/PhysRevB.82.125210 PACS number(s): 71.20.Mq, 84.60.Jt, 71.15.Mb

I. INTRODUCTION

The development and optimization of optoelectronic devices depends crucially on the availability of suitable semiconductor materials. During the last years, there has been a clear trend toward multinary compounds, providing a wider range of electrical, optical, and chemical properties. Obviously, by going from silicon and binary semiconductors such as GaAs to ternary or higher multinary materials, the number of possible compounds grows strongly, providing a great variety of material properties together with a growing difficulty to choose the right one for the respective applications.

A particularly interesting class of ternary materials are half-Heusler compounds with composition *XYZ*. If the elements *X*, *Y*, and *Z* have a total number of eight valence electrons they form a particularly stable ground-state structure. The most electropositive element *X* donates *n* valence electrons to the more electronegative elements *Y* and *Z*. Therefore, a cationic X^{n+} fills the gaps of a covalently bound $(YZ)^{n-}$ sublattice with eight valence electrons. As an intermetallic compound with ionic and covalent bonds the eight-electron half-Heusler material is a ternary Zintl compound.[1] The eight valence electrons of the anionic sublattice act like a closed shell and form a particularly stable configuration. Therefore, the class of eight-electron half-Heusler compounds includes a large number of semiconductors, whose band gaps vary in a wide range.[2] Similar stable eight-electron states cause the band gaps in binary semiconductors of the IV-IV, III-V, II-VI, or I-VII type.

In general, eight-electron half-Heusler materials can be of the I-I-VI, I-II-V, I-III-IV, II-II-IV, and II-III-III type. In this paper, we investigate a set of 648 half-Heusler compounds with the help of all-electron density-functional theory (DFT) calculations. The selection of compounds focuses on materials that are particularly relevant for industrial applications. Therefore, strongly toxic, rare, and heavy elements have been omitted. Pure main group compounds, such as LiAlSi with elements from main groups Ia, IIIa, and IVa, have been investigated as well as compounds with main group elements and transition metals. From the huge class of possible eight-electron half-Heusler compounds, only a very small number has been synthesized up to now. In the I-II-V class, the compounds Li*YZ* with $Y=(Zn,Mg)$ and $Z=(N,P,As)$ have been synthesized and analyzed[3–7] as well as LiAlGe (Ref. 8) and LiCdP.[9] The same compounds have also been investigated with *ab initio* calculations.[10–13] In the I-III-IV class, structural properties of synthesized LiAlSi,[14] LiGaSi,[8] LiGaSn,[15] LiInGe,[16] LiInSn,[16] AuScSn,[17] and AuYPb (Ref. 18) have been reported. Recently, various I-II-V half-Heusler compounds have been studied with the help of density-functional theory and Hartree-Fock methods.[19]

Comparing the structural and electronic properties of the 648 compounds allows to derive global trends for the crystalline structure and the semiconductivity. It should be noted that testing the absolute stability of the half-Heusler phases is beyond the scope of this paper. Thus, for several compounds other phases may be more stable than the half-Heusler phase. Known examples are the compounds NaZn*Z* with $Z=P,As,Sb$, which form a tetragonal Cu_2Sb at ambient conditions while half-Heusler phases become stable only at high pressure.[20]

The obtained data for crystal geometries and band structures can be used to preselect compounds as candidate materials for specific optoelectronic applications. The procedure is used for finding new buffer layer materials for thin film solar cells based on chalcopyrite absorber layers such as $CuInSe_2$ (CISe) or $Cu(In,Ga)Se_2$ (CIGSe). In most high-efficiency thin-film solar cells, the chalcopyrite absorber layer is separated from the ZnO-based window layer by a thin buffer layer. CdS is frequently used as buffer layer material. However, the heavy metal cadmium is harmful for the environment. As more and more large-size solar cells are manufactured, the necessity to find a replacement for cadmium increases. A suitable alternative buffer material must fulfill various criteria: its crystal structure must match well with that of the absorber layer to ensure a good contact. The band gap must be suitably large to avoid absorption losses of the incoming light. At the absorber-buffer interface, the conduction band of the absorber should be close to the Fermi

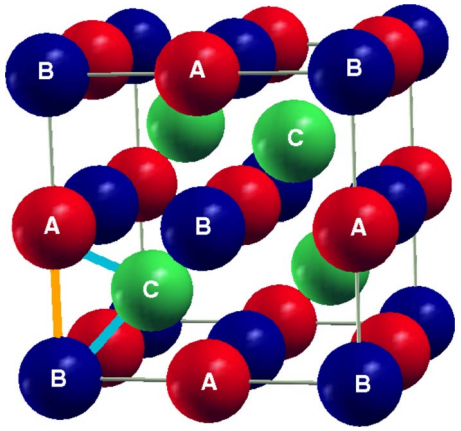

FIG. 1. (Color online) Unit cell of a half-Heusler compound with fcc sublattices A, B, and C. Sublattice C occupies the sparsely filled layers between the NaCl structure formed by sublattices A and B. The closest distance d_{AB} between atoms in sublattice A and B is smaller than corresponding distances $d_{AC}=d_{BC}$ to atoms in lattice site C.

level (inverted interface), and a barrier reduction should be avoided in order to minimize recombination.[21] In this paper, we use the calculated lattice constants and band gaps of half-Heusler materials to select potential substitutes of CdS.

The paper is organized as follows: in Sec. II, the half-Heusler structure is explained. Details on the calculation methods are given in Sec. III. Results for the preferred configurations, the lattice constants, and the band gaps are presented and discussed in Sec. IV. In Sec. V, results are used to select potential buffer layer materials for chalcopyrite solar cells. Some conclusions are drawn in Sec. VI.

II. CRYSTALLINE STRUCTURE

A half-Heusler compound XYZ has a 1:1:1 stoichiometry and a $C1_b$ structure with space group $F\bar{4}3m$. It consists of three nested face-centered-cubic (fcc) sublattices A, B, and C with origins at $\mathbf{r}_A=(0.5,0.5,0.5)$, $\mathbf{r}_B=(0,0,0)$, and $\mathbf{r}_C=(0.25,0.25,0.25)$ in units of the cubic lattice constant a. In contrast to Heusler compounds, there is no sublattice originating from (0.75,0.75,0.75). As a consequence, there is a gap between $\mathbf{r}_A$ and $\mathbf{r}_B$ along the (1,1,1) diagonal axis of the cubic unit cell.

Sublattices A and B together form a NaCl structure. Layers, in which A and B are arranged in a checkerboardlike structure, alternate with sparsely filled layers of the C sublattice. The half-Heusler structure is shown in Fig. 1. It is important to note that the distance $d_{AB}=a/2$ between neighboring atoms of A and B is bigger than the smallest distance $d_{AC}=d_{BC}=\sqrt{3}a/4\simeq 0.433a$ between atoms of A and C or atoms of B and C, respectively. The closest distances between two atoms of the same sublattice is given by $d_{AA}=d_{BB}=d_{CC}=a/\sqrt{2}\simeq 0.71a$.

In general, there are six ways to distribute the elements X, Y, and Z over the sublattices A, B, and C. For symmetry reasons, exchanging the elements on A and B results in a physically equivalent structure. Therefore, only three different configurations have to be distinguished, depending on which component occupies sublattice C. In the following, we denote a specific configuration of a compound XYZ of elements X, Y, and Z by underlining the element on sublattice C. Thus, LiZnP has phosphor on sublattice C.

The electronic structure in the half-Heusler is strongly influenced by the Pauling electronegativity χ of the elements. In the following, we will write components XYZ, ordered by the Pauling negativity, such that $\chi_X\leq\chi_Y\leq\chi_Z$. The electronic structure of LiZnP has been studied by several groups theoretically[10,22] and experimentally.[9,23–25] In LiZnP, the cation Li^+ coexists with a covalently bound $(ZnP)^-$ that forms a zincblende structure. With the extra electron from Li, the zincblende sublattice has eight valence electrons and is particularly stable. As predicted theoretically,[10] the presence of the Li^+ cation shifts the conduction-band states at the X point of the Brillouin zone to higher-energy values. As a consequence, LiZnP has a direct band gap. The effect is characterized by the interstitial insertion rule.[13]

III. CALCULATION METHOD

Properties of eight-electron half-Heusler compounds XYZ are investigated with density-functional theory methods. We apply all-electron calculations with the augmented plane-wave approximation using the program WIEN2K.[26] Calculations for the cubic unit cells of the compounds are performed with 10 000 k points. For all compounds XYZ, the three physically different configurations $XY\underline{Z}$, $X\underline{Y}Z$, and $\underline{X}YZ$ have been considered. For each configuration, we determined the lattice constant a that minimizes the total energy. In a first step, values of a were spread over the reasonable range of the lattice constant. In a second step, a refined grid of test points a in the range of the energy minimum was calculated. Another grid refinement is used in a third step to obtain the optimum lattice constant. The total energies of the configurations $XY\underline{Z}$, $X\underline{Y}Z$, and $\underline{X}YZ$ were compared to determine the most stable configuration. For the geometry optimization, we used the generalized gradient approximation (GGA) of DFT introduced by Perdew, Burke, and Ernzerhof (PBE). With the optimized lattice constant, the band structure was determined with the alternative GGA method proposed by Engel and Vosko (EV-GGA).[27] The EV-GGA is typically less accurate for optimizing the cell parameters[28] but it provides more precise results for nonoccupied states. Especially, the band gap for semiconductors is more accurate. However, it is still distinctly underestimated in many cases, which is a known weakness of DFT methods. A comparison between band gaps calculated with EV-GGA and experimentally measured band gaps is made in Table I.

IV. RESULTS

We have performed a numerical study of eight-electron half-Heusler compounds. Using PBE-GGA for structure optimization and EV-GGA for calculating the band structures we have studied 648 compounds, chosen from the I-I-VI, I-II-V, I-III-IV, II-II-IV, and II-III-III classes.

TABLE I. Comparison of calculated lattice constants a_{calc} and band gaps $E_{gap,\mathrm{EV}}$ with corresponding values from experiments a_{exp} and $E_{gap,exp}$. A hyphen in the last column indicates that no experimental value has been found. All values are rounded to the second decimal. Compounds with As have been added for a more comprehensive comparison. Note that DFT calculations typically underestimate the band gap.

Compound	a_{calc} (Å)	a_{exp} (Å)	$E_{gap,\mathrm{EV}}$ (eV)	$E_{gap,exp}$ (eV)
LiAlGe	6.02	5.96[8]	0.07	
LiAlSi	5.94	5.93[14]	0.12	
LiCdP	6.13	6.10[9]	1.25	
LiGaSi	5.97	6.09[8]	0.20	
LiGaSn	6.41	6.33[15]	0	
LiInGe	6.39	6.30[16]	0	
LiInSn	6.79	6.68[16]	0	
LiMgAs	6.21	6.18[29]	2.30	2.38[29]
LiMgN	5.02	4.99[7]	2.82	3.2[30]
LiMgP	6.02	6.00[31]	2.51	2.43[32]
LiZnAs	5.98	5.94[5]	1.10	1.51[5]
LiZnN	4.93	4.90[6]	0.95	1.91[33]
LiZnP	5.76	5.77[3]	2.14	2.04[23]
AuScSn	6.52	6.42[17]	0.41	
AuYPb	6.83	6.73[18]	0	

A. Configurations

For each compound of elements X, Y, and Z, we have compared the total energies $E(XY\underline{Z})$, $E(X\underline{Y}Z)$, and $E(\underline{X}YZ)$ of the respective configurations. The calculations showed that for a ratio of $r(XY\underline{Z})\simeq 78\%$ of the 648 tested compounds the most stable configuration is the $XY\underline{Z}$. For $r(X\underline{Y}Z)\simeq 17\%$ of all compounds $X\underline{Y}Z$ is most stable, and for less than 5% the most stable configuration is $\underline{X}YZ$.

It is interesting to distinguish between half-Heusler compounds that consist of main group elements only (main) and those that include also transition metals (trans). One example of a *main* compound is the half-Heusler prototype LiAlSi while LiZnP is an example for a *trans* compound. Table II shows the total number of calculated main and trans compounds as well as the respective numbers, separated into compound types I-I-VI, I-II-V, I-III-IV, II-II-IV, and II-III-III. For each half-Heusler type, main and trans, Table II gives the percentage of compounds that favor the $XY\underline{Z}$, $X\underline{Y}Z$, and $\underline{X}YZ$ configuration, respectively. One finds that, altogether, the $XY\underline{Z}$ configuration is favored more often by pure main group compounds (about 86%) than by trans compounds (about 76% of the calculated materials). Remarkably, the $\underline{X}YZ$ is never the most stable configuration for any main compound. Furthermore, in the I-II-V and the II-II-IV class all tested main compounds favor the $XY\underline{Z}$ configuration. In the I-I-VI and the II-III-III class, there are specially high ratios of trans compounds that favor the $XY\underline{Z}$ configuration.

The fact that $XY\underline{Z}$ is energetically favorable in most cases while $\underline{X}YZ$ is rarely favored can be understood as follows: typically, the half-Heusler compound in the $XY\underline{Z}$ configuration forms an anionic $(YZ)^{n-}$ zincblende structure with Y and Z on sublattice B and C, respectively, that is filled with X^{n+} cations on sublattice A.[2] The distance d_{XY} between the elements X and Y is larger than the distances $d_{XZ}=d_{YZ}$. A close distance between Y and Z favors the formation of stable covalent bonds between the two elements. A close distance between the cationic X^{n+} and the most electronegative element Z reduces the local electric dipoles and the corresponding energy contributions. In the $\underline{X}YZ$ structure, there is a larger distance between X^{n+} and the most anionic Z, leading to a larger dipole. The $\underline{X}YZ$ structure separates the partners of the covalent bonds, which turns out to be strongly disadvantageous in most cases.

If the difference $\chi_Z-\chi_Y$ is small, the dipole energy difference between the $XY\underline{Z}$ configuration with a larger distance d_{XY} and the $X\underline{Y}Z$ configuration with a larger distance d_{XZ} is of less relevance. Indeed, our results show that compounds favoring the $X\underline{Y}Z$ configuration have an average value $(\chi_Z-\chi_Y)_{av}^{X\underline{Y}Z}\simeq 0.35$ that is distinctly smaller than $(\chi_Z-\chi_Y)_{av}^{XY\underline{Z}}\simeq 0.63$. If $\chi_Z-\chi_X$ is small, all electronegativities χ_X, χ_Y, and χ_Z are of comparable size. According to this, the average value of $(\chi_Z-\chi_X)_{av}^{XY\underline{Z}}\simeq 0.64$ for compounds favoring $\underline{X}YZ$ is considerably below $(\chi_Z-\chi_X)_{av}^{XY\underline{Z}}\simeq 1.15$. This means that the $\underline{X}YZ$ configuration is typically most stable if the cationic character of X is less pronounced and the bond between Y and Z is comparably weak in any configuration. In Fig. 2 the obtained values for $\chi_Z-\chi_X$ and $\chi_Z-\chi_Y$ are shown for compounds favoring the $XY\underline{Z}$, $X\underline{Y}Z$, and the $\underline{X}YZ$ configuration, respectively.

TABLE II. Number of calculated half-Heusler materials of type I-I-VI, I-II-V, I-III- IV, II-II-IV, and II-III-III, divided into compounds that consist of main group elements only (main) and those that include transition metals (trans). For all half-Heusler types, the values of $r(XY\underline{Z})$, $r(X\underline{Y}Z)$, and $r(\underline{X}YZ)$ denote the respective percentage of compounds that favor configuration $XY\underline{Z}$, $X\underline{Y}Z$, and $\underline{X}YZ$, respectively. The quantity r(semi) denotes the percentage of semiconducting materials for the respective half-Heusler type.

	I-I-VI		I-II-V		I-III-IV		II-II-IV		II-III-III		All	
Type	main	trans	main	trans	main	trans	main	trans	main	trans	main	trans
N_{comp}	18	44	32	121	75	200	30	73	22	33	177	471
$r(XY\underline{Z})$	83.3%	81.8%	100.0%	77.7%	74.7%	73.0%	100.0%	69.9%	86.4%	97.0%	85.9%	76.2%
$r(X\underline{Y}Z)$	16.7%	13.6%	0.0%	17.4%	25.3%	17.5%	0.0%	26.0%	13.6%	3.0%	14.1%	17.4%
$r(\underline{X}YZ)$	0.0%	4.5%	0.0%	5.0%	0.0%	9.5%	0.0%	4.1%	0.0%	0.0%	0.0%	6.4%
r(semi)	100.0%	40.9%	100.0%	21.5%	24.0%	34.0%	93.3%	12.3%	63.6%	39.4%	62.1%	28.5%

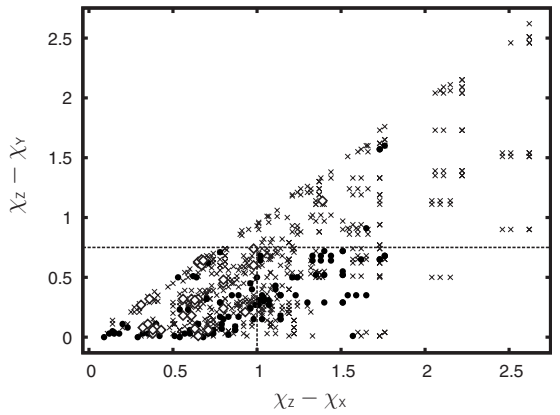

FIG. 2. Differences of the Pauling negativities $\chi_Z-\chi_X$ of elements X and Z and $\chi_Z-\chi_Y$ of elements Y and Z for all compounds XYZ. Values are shown for compounds favoring the $XY\underline{Z}$ (×), the $X\underline{Y}Z$ (●), and the $\underline{X}YZ$ (◇) configuration, where the underlined element occupies sublattice C. For most of the $X\underline{Y}Z$ and $\underline{X}YZ$ compounds, the difference $\chi_Z-\chi_Y$ is below 0.75 (horizontal line). For almost all $\underline{X}YZ$ compounds, the difference $\chi_Z-\chi_X$ is below 1 (vertical line). Note that the components XYZ are sorted such that $\chi_X \leq \chi_Y \leq \chi_Z$.

Many eight-electron half-Heusler compounds are semiconductors because of the stable configuration formed by the valence electrons in the $(YZ)^-$ sublattice. Using EV-GGA, we have calculated the band structures of all compounds.

B. Lattice constants

The lattice constant has been optimized for all compounds in all three configurations. In the following, the *lattice constant of a compound* refers to the optimized lattice constant of the most stable half-Heusler configuration of this compound. Calculated lattice constants are compared with known experimental values in Table I. Complete lists of lattice constants for calculated half-Heusler compounds of type I-I-VI, I-II-V, I-III-IV, II-II-IV, and II-III-III are given in Tables III–VII. We restrict the analysis of the lattice constants on compounds with stable $XY\underline{Z}$ configuration, which enables a reasonable comparison of the geometric properties. It is instructive to discuss the optimized lattice constants a as a function of the atomic radii r_X, r_Y, and r_Z. A widely used set of atomic radii for elements in crystals has been determined phenomenologically by Slater.[34] In a first step, we assume that the shortest atom distances $d_{XZ}=d_{YZ}$ have the strongest influence on the unit-cell size. From the definition of the Slater radii one expects that, in the absence of other constraints, the optimum distance d_{XZ} of atoms X and Z is approximately r_X+r_Z. However, in most cases, elements X and Y with $\chi_X<\chi_Y$ have different radii $r_X>r_Y$ so that $d_{XZ}=r_X+r_Z$ and $d_{YZ}=r_Y+r_Z$ cannot be satisfied at the same time. As shown in Fig. 3, the distances $d_{XZ}=d_{YZ}=\frac{\sqrt{3}}{4}c$ are typically smaller than r_X+r_Z but larger than r_Y+r_Z. One finds that deviations in both directions are of the same order. In fact, the equilibrium lattice constant can be approximated by the arithmetic mean of $\frac{4}{\sqrt{3}}(r_X+r_Z)$ and $\frac{4}{\sqrt{3}}(r_Y+r_Z)$ as shown in Fig. 4. Note that the resulting relation

$$a \simeq f_1 \equiv \frac{2}{\sqrt{3}}(r_X + r_Y + 2r_Z) \tag{1}$$

does not include any fit parameter and the average relative deviation between f_1 and the calculated lattice constant a is below 5%.

Let us consider a notional mechanical analogon of the half-Heusler crystals, in which the distances d_{XZ} and d_{YZ} are controlled by ideal linear springs with an equilibrium length of r_X+r_Z and r_Y+r_Z, respectively. The expression in Eq. (1) would provide the geometrically optimum configuration if the springs would have the same strength. We can now think of a more refined virtual model system in which centers of neighboring atom pairs XY, XZ, and YZ are connected by springs of different strengths and equilibrium lengths r_X+r_Y, r_X+r_Z, and r_Y+r_Z, respectively. With $a=2d_{XY}=\frac{4}{\sqrt{3}}d_{XZ}=\frac{4}{\sqrt{3}}d_{YZ}$, the optimum lattice constant a results from the combination of three phenomenological harmonic potentials for d_{XY}, d_{XZ}, and d_{YZ} with individual potential strengths k_{XY}, k_{XZ}, and k_{YZ},

TABLE III. Equilibrium lattice constants a for I-I-VI half-Heusler compounds. In the energetically favored configuration, the underlined element occupies sublattice C.

Name	a (Å)	Name	a (Å)	Name	a (Å)	Name	a (Å)	Name	a (Å)	Name	a (Å)
AgAuO	5.792	KAuO	6.206	KNaSe	7.334	LiCuS	5.594	NaLiO	5.239	RbCuSe	6.846
AgAuS	6.219	KAuS	6.740	KRbO	6.734	LiCuSe	5.870	NaLiS	6.223	RbLiO	6.179
AgAuSe	6.407	KAuSe	6.923	KRbS	7.712	NaAgO	5.696	NaLiSe	6.500	RbLiS	6.686
CuAgO	5.899	KCuO	5.864	KRbSe	7.960	NaAgS	6.334	RbAgO	6.410	RbLiSe	6.868
CuAgS	5.961	KCuS	6.400	LiAgO	5.409	NaAgSe	6.539	RbAgS	7.064	RbNaO	6.420
CuAgSe	6.081	KCuSe	6.593	LiAgS	6.026	NaAuO	5.803	RbAgSe	7.278	RbNaS	7.338
CuAuS	5.966	KLiO	5.888	LiAgSe	6.259	NaAuS	6.299	RbAuO	6.443	RbNaSe	7.608
CuAuSe	6.098	KLiS	6.849	LiAuO	5.490	NaAuSe	6.510	RbAuS	7.000		
KAgO	6.165	KLiSe	6.656	LiAuS	6.006	NaCuO	5.338	RbAuSe	7.177		
KAgS	6.801	KNaO	6.147	LiAuSe	6.214	NaCuS	6.021	RbCuO	5.984		
KAgSe	7.010	KNaS	7.089	LiCuO	4.990	NaCuSe	6.143	RbCuS	6.666		

TABLE IV. Equilibrium lattice constants a for I-II-V half-Heusler compounds. In the energetically favored configuration, the underlined element occupies sublattice C.

Name	a (Å)	Name	a (Å)	Name	a (Å)	Name	a (Å)	Name	a (Å)	Name	a (Å)
BaAgN	6.430	CaPAu	6.421	KSrN	6.567	MgPAu	6.107	RbBaP	7.817	SrCuP	6.574
BaAgP	7.052	CaVAg	6.662	KSrP	7.445	MgVAg	6.165	RbBaV	8.378	SrLiN	5.932
BaAuN	6.470	CaVAu	6.588	KSrV	8.184	MgVCu	5.881	RbCaN	6.536	SrLiNb	7.018
BaCuN	6.246	CaVCu	6.390	KVCd	6.867	NaCaN	5.885	RbCaNb	8.060	SrLiP	6.824
BaCuP	6.723	CdAgN	5.777	KVZn	6.889	NaCaNb	7.208	RbCaP	7.409	SrLiV	6.970
BaLiN	6.250	CdAgP	6.289	KZnN	5.972	NaCaP	6.790	RbCaV	8.062	SrNbAg	6.975
BaLiNb	7.064	CdAuN	5.822	KZnP	6.668	NaCaV	7.375	RbCdN	6.493	SrNbCu	6.720
BaLiP	7.144	CdCuN	5.502	LiCaN	5.572	NaCdN	5.706	RbCdP	7.130	SrPAu	6.694
BaLiV	7.055	CdCuP	6.036	LiCaP	6.506	NaCdP	6.440	RbMgN	6.321	SrVAg	6.934
BaNaN	6.468	CdPAu	6.276	LiCaV	6.660	NaMgN	5.460	RbMgNb	7.289	SrVAu	6.863
BaNaNb	7.535	KBaN	6.762	LiCdN	5.383	NaMgP	6.376	RbMgP	7.097	SrVCu	6.670
BaNaP	7.343	KBaNb	7.801	LiCdP	6.134	NaMgV	6.747	RbMgV	7.408	VCdAg	6.022
BaNaV	7.460	KBaP	7.658	LiMgN	5.018	NaNbCd	6.651	RbNbCd	7.176	VCdAu	6.235
BaNbAg	6.937	KBaV	8.193	LiMgP	6.019	NaNbZn	6.326	RbNbZn	7.062	VCdCu	5.922
BaNbCu	6.866	KCaN	6.330	LiMgV	6.047	NaSrN	6.190	RbSrN	6.751	VZnAg	5.986
BaPAu	6.987	KCaNb	8.137	LiVCd	5.947	NaSrNb	7.389	RbSrNb	8.294	VZnAu	5.993
BaVAg	6.888	KCaP	7.207	LiVZn	5.807	NaSrP	7.068	RbSrP	7.623	VZnCu	5.648
BaVAu	6.703	KCaV	7.888	LiZnN	4.927	NaSrV	7.345	RbSrV	8.326	ZnAgN	5.496
BaVCu	6.875	KCdN	6.200	LiZnP	5.757	NaVCd	6.589	RbVCd	7.166	ZnAgP	6.021
CaAgN	5.849	KCdP	6.875	MgAgN	5.524	NaVZn	6.254	RbVZn	6.959	ZnAuN	5.555
CaAgP	6.478	KMgN	6.025	MgAgP	6.141	NaZnN	5.360	RbZnN	6.302	ZnCuN	5.306
CaAuN	5.895	KMgNb	7.313	MgAuN	5.586	NaZnP	6.149	RbZnP	6.958	ZnCuP	5.700
CaCuN	5.592	KMgP	6.841	MgCuN	5.165	NbCdCu	6.050	SrAgN	6.134	ZnPAu	6.016
CaCuP	6.260	KMgV	7.277	MgCuP	5.850	NbZnCu	5.813	SrAgP	6.755		
CaNbAg	6.721	KNbCd	7.134	MgNbAg	6.323	RbBaN	6.917	SrAuN	6.173		
CaNbCu	6.472	KNbZn	6.856	MgNbCu	6.020	RbBaNb	8.816	SrCuN	5.929		

$$U(a) \equiv k_{XY}\left(r_X + r_Y - \frac{1}{2}a\right)^2 + k_{XZ}\left(r_X + r_Z - \frac{\sqrt{3}}{4}a\right)^2 + k_{YZ}\left(r_Y + r_Z - \frac{\sqrt{3}}{4}a\right)^2. \quad (2)$$

Taking the minimum of U provides the relation

$$a \simeq f_2 \equiv \frac{4}{4k_{XY} + 3k_{XZ} + 3k_{YZ}}[2k_{XY}(r_X + r_Y) + \sqrt{3}k_{XZ}(r_X + r_Z) + \sqrt{3}k_{YZ}(r_Y + r_Z)]. \quad (3)$$

Fitting the parameters with the calculated data gives $k_{XZ} \approx 1.11k_{XY}$ and $k_{YZ} \approx 1.31k_{XY}$ (see Fig. 4). With these values, the relative deviation $|f_2 - a|/a$ is on average 3.0%. The largest potential strength k_{YZ} regulates the distance between the Y and the Z component. This means that the stiffest interatomic bond is the covalent bond, followed by the ionic bond between X and Z. It is noteworthy that within this picture the phenomenological potential for the distance between X and Y is not much weaker than that for d_{XZ}.

C. Band gap

The band structures of the optimized compounds have been calculated with EV-GGA and PBE-GGA. A comparison of the obtained band gaps $E_{gap,\mathrm{EV}}$ and $E_{gap,\mathrm{PBE}}$ with existing experimental results $E_{gap,exp}$ shows that band gaps obtained with EV-GGA are always more accurate than those found with PBE-GGA. Band gaps calculated with EV-GGA are compared with existing experimental band gaps in Table I. In the case of LiMgP, LiZnP, and LiMgAs, $E_{gap,\mathrm{EV}}$ differs less than 6% from the experimental values. However, the calculated band gap for LiZnAs is 32% smaller than the experimental value and in the case of LiZnN, $E_{gap,\mathrm{EV}}$ is only half as big as $E_{gap,exp}$. In general, the relative deviation $q_{gap} \equiv (E_{gap,exp} - E_{gap,\mathrm{EV}})/E_{gap,exp}$ is in the range of $-3\% \leq q_{gap} \leq 50\%$. This allows us to use the calculated values as an approximate lower bound of the real band gap. Especially, all compounds with a finite $E_{gap,\mathrm{EV}}$ can be considered as semiconductors.

TABLE V. Equilibrium lattice constants a for I-III-IV half-Heusler compounds. In the energetically favored configuration, the underlined element occupies sublattice C.

Name	a (Å)	Name	a (Å)	Name	a (Å)	Name	a (Å)	Name	a (Å)	Name	a (Å)
AgBC	5.085	KBC	5.641	LiGeB	5.163	NaGeB	5.608	RbHfB	6.507	TiAgB	5.523
AgGeB	5.632	KBPb	6.639	LiHfAl	6.087	NaHfAl	6.741	RbHfSc	7.687	TiAlAg	6.126
AlAgC	5.430	KGaC	6.096	LiHfB	5.520	NaHfB	5.878	RbInC	6.641	TiAlAu	6.111
AlAgGe	6.201	KGaGe	6.889	LiHfGa	6.242	NaHfGa	6.584	RbInGe	7.353	TiAlCu	5.827
AlAgSn	6.463	KGaPb	7.301	LiHfIn	6.392	NaHfIn	6.923	RbInSi	7.248	TiBAu	5.535
AlAuC	5.484	KGaSi	6.770	LiHfSc	6.497	NaHfSc	6.940	RbInSn	7.579	TiCuB	5.245
AlCuC	5.047	KGaSn	7.133	LiInGe	6.390	NaInGe	6.695	RbScC	6.380	TiGaAg	6.121
AlCuGe	5.831	KGeB	6.195	LiInPb	6.936	NaInPb	7.244	RbScGe	7.345	TiGaAu	6.104
AlCuSi	5.685	KHfB	6.328	LiInSi	6.272	NaInSi	6.582	RbScSi	7.274	TiGaCu	5.788
AlGeAu	6.166	KHfSc	7.557	LiInSn	6.794	NaInSn	7.077	RbScTi	7.697	YAgC	5.889
AlPbAu	6.566	KInC	6.326	LiScC	5.324	NaScC	5.687	RbSiB	6.410	YAgGe	6.564
AlSiAg	6.072	KInGe	7.109	LiScGe	6.311	NaScGe	6.646	RbSnB	6.763	YAgPb	6.854
AlSiAu	6.032	KInPb	7.601	LiScPb	6.789	NaScPb	7.109	RbTiAl	7.113	YAgSn	6.750
AlSnAu	6.432	KInSi	7.004	LiScSi	6.272	NaScSi	6.607	RbTiB	6.476	YAuC	5.910
BAuC	5.201	KInSn	7.465	LiScSn	6.333	NaScSn	7.043	RbTiGa	6.986	YCuC	5.660
CuBC	4.612	KScC	6.182	LiScTi	6.360	NaScTi	6.801	RbTiIn	7.301	YCuGe	6.244
CuGeB	5.260	KScGe	7.127	LiSiB	5.008	NaSiB	5.477	RbYC	6.555	YCuPb	6.601
CuSiB	5.089	KScPb	7.587	LiTiAl	5.895	NaSnB	5.950	RbYGe	7.526	YCuSi	6.174
GaAgC	5.541	KScSi	7.073	LiTiB	5.279	NaTiAl	6.606	RbYHf	7.940	YCuSn	6.495
GaAgGe	6.287	KScSn	7.507	LiTiGa	6.055	NaTiB	5.712	RbYSi	7.462	YGeAu	6.535
GaAgSn	6.533	KScTi	7.494	LiTiIn	6.124	NaTiGa	6.452	RbYTi	7.856	YHfAu	6.799
GaAuC	5.591	KSiB	6.068	LiYC	5.692	NaTiIn	6.824	RbYZr	8.012	LiZrSc	6.830
GaCuC	5.150	KSnB	6.465	LiYGe	6.614	NaYC	5.983	RbZrAl	7.397	YSiAg	6.499
GaCuGe	5.900	KTiAl	7.139	LiYHf	6.752	NaYGe	6.896	RbZrB	6.552	YSiAu	6.460
GaCuSi	5.748	KTiB	6.258	LiYPb	7.064	NaYHf	7.448	RbZrGa	7.280	YSnAu	6.729
GaGeAu	6.243	KTiGa	7.002	LiYSi	6.577	NaYPb	7.338	RbZrIn	7.428	YTiAg	6.710
GaSiAg	6.117	KTiIn	7.152	LiYSn	6.581	NaYSi	6.858	RbZrSc	7.946	YTiAu	6.688
GaSiAu	6.106	KYC	6.389	LiYTi	6.627	NaYSn	7.280	ScAgC	5.600	YTiCu	6.452
GaSnAu	6.533	KYGe	7.333	LiYZr	6.789	NaYTi	7.041	ScAgGe	6.300	YZrAg	6.861
GeBAu	5.675	KYSi	7.281	LiZrAl	6.082	NaZrAl	6.766	ScAgPb	6.645	YZrAu	6.822
HfAgB	5.732	KYSn	7.693	LiZrB	5.575	NaZrB	5.916	ScAgSn	6.506	YZrCu	6.608
HfAlAu	6.305	KYTi	7.737	LiZrGa	6.275	NaZrGa	6.609	ScAuC	5.631	ZrAgB	5.768
HfAlCu	6.012	KYZr	7.910	LiZrIn	6.286	NaZrIn	6.962	ScCuC	5.326	ZrAlAg	6.330
HfBAu	5.741	KZrIn	7.424	LiZrSc	6.521	RbAlC	6.364	ScCuGe	5.969	ZrAlAu	6.311
HfCuB	5.486	KZrSc	7.621	NaAlC	5.401	RbAlGe	7.122	ScCuSi	5.888	ZrAlCu	6.049
HfGaAg	6.270	LiAlC	4.924	NaAlGe	6.383	RbAlPb	7.511	ScCuSn	6.246	ZrBAu	5.774
InAgGe	6.504	LiAlGe	6.019	NaAlPb	6.901	RbAlSi	7.018	ScGeAu	6.286	ZrCuB	5.528
InAgSn	6.728	LiAlPb	6.594	NaAlSi	6.287	RbAlSn	7.346	ScPbAu	6.621	ZrGaAg	6.306
InCuGe	6.294	LiAlSi	5.937	NaAlSn	6.729	RbBC	6.047	ScSiAg	6.224	ZrGaAu	6.331
InGeAu	6.492	LiAlSn	6.464	NaBC	4.850	RbBPb	6.915	ScSiAu	6.209	ZrGaCu	6.007
InPbAu	6.930	LiBC	4.243	NaBPb	6.154	RbGaC	6.450	ScSnAu	6.526	ZrInAg	6.528
KAlC	6.018	LiGaC	4.986	NaGaC	5.451	RbGaGe	7.164	ScTiAg	6.466	ZrInAu	6.526
KAlGe	6.842	LiGaGe	6.032	NaGaGe	6.411	RbGaPb	7.526	ScTiAu	6.424	ZrScAg	6.641
KAlPb	7.295	LiGaPb	6.605	NaGaPb	6.896	RbGaSi	7.050	ScTiCu	6.188	ZrScAu	6.604
KAlSi	6.731	LiGaSi	5.969	NaGaSi	6.284	RbGaSn	7.375	SiAgB	5.462	ZrScCu	6.378
KAlSn	7.104	LiGaSn	6.412	NaGaSn	6.716	RbGeB	6.523	SiBAu	5.501		

TABLE VI. Equilibrium lattice constants a for II-II-IV half-Heusler compounds. In the energetically favored configuration, the underlined element occupies sublattice C.

Name	a (Å)	Name	a (Å)	Name	a (Å)	Name	a (Å)	Name	a (Å)	Name	a (Å)
BaCaC	6.748	BaMgSi	7.282	CaCdPb	7.160	HfMgCd	6.628	SrCaPb	7.886	SrTiCd	7.255
BaCaGe	7.719	BaMgSn	7.691	CaCdSi	6.697	HfMgZn	6.334	SrCaSi	7.415	SrTiZn	6.964
BaCaHf	8.025	BaMgTi	7.325	CaCdSn	7.122	HfZnCd	6.307	SrCaSn	7.816	SrZnC	6.096
BaCaPb	8.129	BaSrC	6.930	CaHfCd	7.060	MgCdC	5.654	SrCaTi	7.943	SrZnGe	6.855
BaCaSi	7.714	BaSrGe	7.921	CaHfMg	7.217	MgCdGe	6.486	SrCdC	6.311	SrZnPb	7.129
BaCaSn	8.053	BaSrHf	8.288	CaHfZn	6.793	MgCdPb	6.952	SrCdGe	7.036	SrZnSi	6.778
BaCaTi	7.921	BaSrPb	8.343	CaMgC	5.909	MgCdSi	6.386	SrCdPb	7.389	SrZnSn	6.994
BaCdC	6.643	BaSrSi	8.110	CaMgGe	6.799	MgCdSn	6.851	SrCdSi	6.964	TiZnCd	6.159
BaCdGe	7.318	BaSrSn	8.268	CaMgPb	7.239	MgTiCd	6.491	SrCdSn	7.261	ZnCdC	5.583
BaCdPb	7.639	BaTiCd	7.187	CaMgSi	6.365	MgTiZn	6.178	SrHfCd	7.314	ZnCdGe	6.305
BaCdSi	7.242	BaTiZn	7.173	CaMgSn	7.165	MgZnC	5.300	SrHfMg	7.448	ZnCdPb	6.721
BaCdSn	7.524	BaZnC	6.459	CaMgTi	7.129	MgZnGe	6.215	SrHfZn	7.035	ZnCdSi	6.229
BaHfCd	7.496	BaZnGe	7.166	CaTiCd	6.961	MgZnPb	6.627	SrMgC	6.235	ZnCdSn	6.594
BaHfMg	7.388	BaZnPb	7.390	CaTiZn	6.690	MgZnSi	6.120	SrMgGe	7.068		
BaHfZn	7.204	BaZnSi	7.084	CaZnC	5.745	MgZnSn	6.465	SrMgPb	7.502		
BaMgC	6.557	BaZnSn	7.276	CaZnPb	6.877	SrCaC	6.571	SrMgSi	7.012		
BaMgGe	7.346	CaCdC	6.008	CaZnSi	6.482	SrCaGe	7.459	SrMgSn	7.427		
BaMgPb	7.778	CaCdGe	6.771	CaZnSn	7.331	SrCaHf	8.241	SrMgTi	7.419		

In Table II, the percentages of semiconducting materials are given for main and trans compounds of all half-Heusler types. One finds that a rate of 62.1% of main compounds are semiconducting while only 28.5% of the calculated trans compounds have a finite band gap. Remarkably, all main compounds of type I-I-VI and I-II-V and nearly all II-II-IV main compounds are semiconductors. On the other hand, only 24% of the I-III-IV main compounds have a calculated band gap $E_{gap,\mathrm{EV}}>0$. Particularly large rates of semiconducting trans compounds exist in the I-I-VI and the II-III-III class.

There is a strong correlation between the stability of the XYZ configuration and semiconductivity. In classes I-II-V and II-II-IV, all compounds favor the XYZ configuration and nearly all compounds are semiconducting. For trans compounds, the classes I-I-VI and II-III-III have the highest rates of XYZ stability and the highest rates of semiconductivity. In Fig. 5, the calculated band gaps are shown as a function of $\Delta E=E_{XYZ}-E_{XYZ}$ and $\Delta E=E_{XYZ}-E_{XYZ}$, respectively. Consequently, compounds with negative ΔE favor the XYZ or the XYZ configuration. It turns out that only a small fraction of these compounds are semiconducting. This means, compounds that favor XYZ or XYZ states do not form a particularly stable eight-electron substructure in any configuration. For the small number of semiconductors that favor the XYZ, the energy difference $|E_{XYZ}-E_{XYZ}|$ is comparably low. From the compounds with a finite calculated band gap, more than 93% favor the XYZ configuration. The calculated band gaps

TABLE VII. Equilibrium lattice constants a for II-III-III half-Heusler compounds. In the energetically favored configuration, the underlined element occupies sublattice C.

Name	a (Å)	Name	a (Å)	Name	a (Å)	Name	a (Å)	Name	a (Å)	Name	a (Å)
BaAlB	6.626	BaYAl	7.700	CaScAl	7.099	MgGaB	5.497	SrInB	6.497	YMgAl	6.865
BaAlGa	7.212	BaYB	6.884	CaScB	6.280	MgInGa	6.558	SrInGa	7.078	YMgB	6.109
BaAlIn	7.377	BaYGa	7.567	CaScGa	6.948	MgScAl	6.629	SrScAl	7.406	YMgGa	6.727
BaGaB	6.631	BaYIn	7.910	CaScIn	7.248	MgScB	5.814	SrScB	6.539	YMgIn	7.045
BaInB	6.830	CaAlB	5.940	CaYAl	7.431	MgScGa	6.478	SrScGa	7.193	YMgSc	7.206
BaInGa	7.353	CaAlGa	6.583	CaYB	6.520	MgScIn	6.814	SrScIn	7.364		
BaScAl	7.512	CaAlIn	6.880	CaYGa	7.167	SrAlB	6.287	SrYAl	7.275		
BaScB	6.706	CaGaB	5.919	CaYIn	7.478	SrAlGa	6.877	SrYB	6.728		
BaScGa	7.394	CaInB	6.187	MgAlB	5.507	SrAlIn	7.159	SrYGa	7.410		
BaScIn	7.740	CaInGa	6.810	MgAlGa	6.260	SrGaB	6.265	SrYIn	7.714		

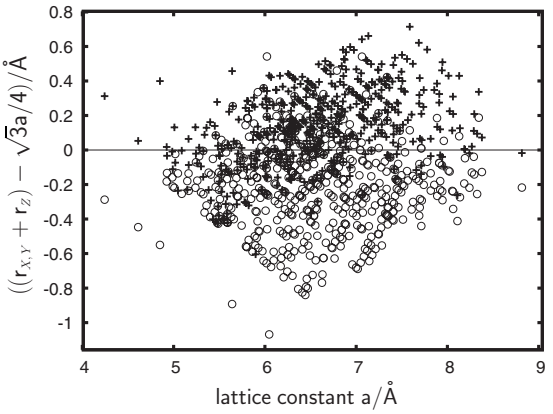

FIG. 3. The sum of Slater radii r_j+r_Z of elements $j=X$, Y, and Z should be comparable to the distance $d_{jZ}=\sqrt{3}a/4$. The figure shows $(r_X+r_Z)-\sqrt{3}a/4$ (+), which is larger than zero in most cases, and $(r_Y+r_Z)-\sqrt{3}a/4$ (○), which is typically smaller than zero. Data are shown for compounds favoring the XYZ configuration.

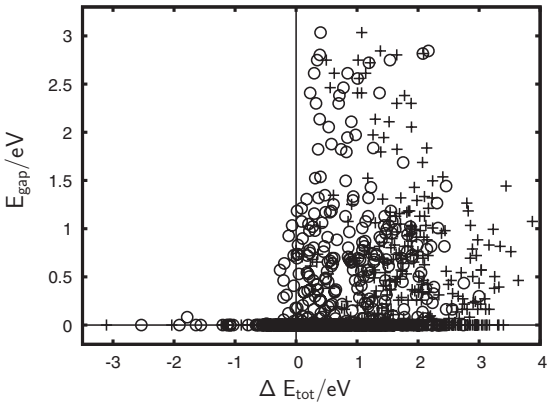

FIG. 5. Calculated band gaps for the stable configuration among compounds XYZ as a function of the differences of total energies $\Delta E=E_{\underline{X}YZ}-E_{XY\underline{Z}}$ (○) and $\Delta E=E_{\underline{X}YZ}-E_{X\underline{Y}Z}$ (+). Negative ΔE correspond to compounds favoring $\underline{X}YZ$ or $X\underline{Y}Z$ while E_{XYZ} is more stable for $\Delta E>0$. Note that DFT calculations typically underestimate the band gap.

cover the range from 0 to 3 eV continuously without essential interruptions. Thus, eight-electron half-Heusler compounds can be used for a wide range of applications and a suitable half-Heusler compound can be found for practically all desired band gaps.

V. NEW BUFFER MATERIALS FOR CHALCOPYRITE SOLAR CELLS

The obtained results for the half-Heusler compounds can be used to select materials for specific applications. One interesting example is the buffer layer in thin film solar cells with a chalcopyrite absorption layer. Up to now the record efficiency of 20.1% has been found for thin-film solar cells with a p-type $Cu(In,Ga)Se_2$ absorption layer, separated from the n-type ZnO window layer by a buffer layer made of CdS.[35] There must be a good geometrical matching between the absorber and the buffer layer in order to avoid interface defects. The buffer material must have a band gap of at least 2 eV so that the light absorption in the buffer layer is reasonably small. Furthermore, carrier recombinations at the interface should be minimized.[21] CdS satisfies these criteria but there are strong efforts to find a less toxic buffer material (see Refs. 36–38 and references therein).

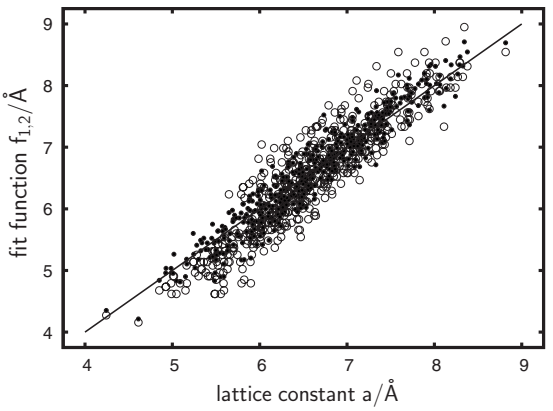

FIG. 4. Fit functions f_1 (○) and f_2 (●) of the lattice constant a, plotted over a. Functions f_1 and f_2 are defined in Eqs. (1) and (3), respectively. Data are shown for compounds favoring the XYZ configuration. The diagonal line corresponds to a perfect match.

The class of eight-electron half-Heusler compounds includes a huge number of compounds, many of which are semiconductors. Therefore, a proper selection of promising materials must be made before a suitable set of compounds can be synthesized and tested experimentally. Our *ab initio* results are used to select half-Heusler compounds that fulfill two relevant criteria: The band gap must be larger than 2 eV and the lattice structure must match properly with that of the absorber layer.

The most relevant chalcopyrite materials for photovoltaic applications are of the type $CuIn_{1-x}Ga_xSe_{2-y}S_y$ with $0 \le x \le 1$ and $0 \le y \le 2$. For $x=0$ and $y=0$, one has CISe, which is chosen as a reference absorber material in the following. The tetragonal unit cell of CISe is shown in Figs. 6(a) and 6(b). The comparison with the structure of a half-Heusler-type LiZnP in Figs. 6(c) and 6(d) shows that there is a good geometrical matching if the lattice constant a of the half-Heusler is similar to the small lattice constant a of the $CuInSe_2$, which is approximately $a \simeq 5.8$ Å.[39,40] The lattice structure of CISe matches well with that of CdS having lattice constants a and c with $\sqrt{2}a \simeq 5.85$ Å in the wurtzite phase[41] and a lattice constant $a \simeq 5.84$ Å in the zinc blende phase.[42] $CuGaSe_2$ has a small lattice constant of $a \simeq 5.61$ Å, for $CuInS_2$ a value of $a \simeq 5.52$ Å has been measured.[40] Though the lattice constants of $CuInS_2$ and CdS differ by approximately 5%, respectable efficiencies of up to 13% have been reported for thin film solar cells with a $CdS/CuInS_2$ junction.[43] We conclude that a proper lattice matching is important but lattice constant differences of a few percent are tolerable. Therefore, we choose as a minimum criterion that the lattice constant a of a potential buffer material should deviate less than 0.4 Å from the value of 5.8 Å.

In Fig. 7, calculated band gaps and lattice constants are shown for all investigated half-Heusler compounds. Potential buffer materials are located within the framed area. Band-

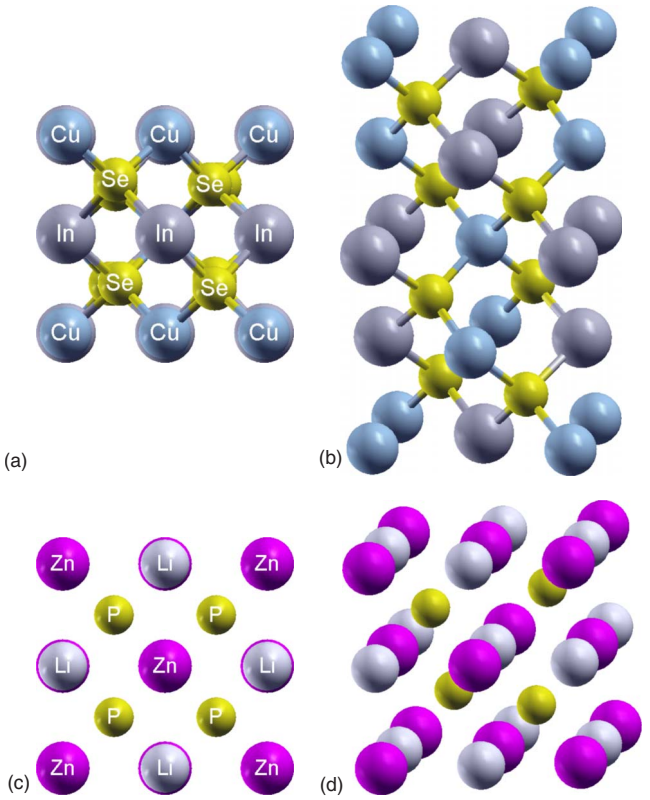

FIG. 6. (Color online) Structural similarity between chalcopyrite and half-Heusler materials. (a) Top view and (b) perspective side view on the tetragonal unit cell of the absorber material $CuInSe_2$; (c) top view and (d) perspective side view on the half-Heusler material LiZnP.

gap values calculated with EV-GGA are typically smaller than the experimentally measured band gaps. Comparisons with measured band gaps show that calculated band gaps can be up to 50% smaller than the corresponding experimental value, see Table I. In order to make sure that all relevant

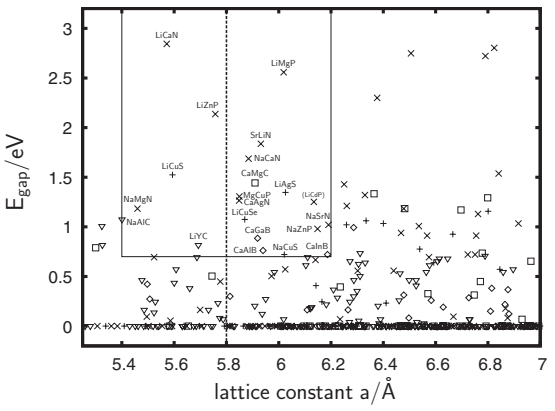

FIG. 7. Diagram of lattice constants a and calculated band gaps E_{gap} of half-Heusler compounds in the range of $5.3 \leq a \leq 7$ Å and $E_{gap} < 3.2$ eV. Note that DFT calculations typically derestimate the band gap. The dashed vertical line denotes the small compounds located within the thin black frame are candidates for substituting CdS in the buffer layer of chalcopyrite solar cells. The dashed vertical line denotes the small lattice constant of $CuInSe_2$.

materials are included in our list of candidate materials, we choose a suitably small lower boundary for the band gap calculated with EV-GGA, namely, $E_{gap,\mathrm{EV}} > 0.7$ eV. With the chosen criteria, a small set of 20 compounds out of 648 investigated eight-electron half-Heusler materials have been selected. All other calculated compounds can be excluded as CdS substitute but they may be suited for many other optoelectronic applications. The properties of the small set of potential buffer materials can be studied in detail experimentally. Suitable buffer material candidates are LiCuS, NaCuS, NaAgS, and LiCuSe from the I-I-VI group. The largest number of potential buffer materials are found in the I-II-V group, namely, NaMgN, CaAgN, LiMgP, and MgCuP as well as XCaN, XSrN, and XZnP with X=Li,Na. Furthermore, there is NaAlC and LiYC from the I-III-IV group, CaMgC from the II-II-IV group, and CaXB with X=Al,Ga,In from the II-III-III group. The optimum buffer material depends on the chosen absorber material and its lattice constant. Recently, thin films of LiCuS and LiZnP have been successfully sputtered on a CIGSe layer.[44] In both cases, a mechanically stable contact with the chalcopyrite material and a band gap of approximately 2 eV have been measured. This indicates that the criteria tested with the calculated data are indeed successfully fulfilled. Further measurements remain to be done.

VI. CONCLUSIONS

The class of eight-electron half-Heusler materials includes a large number of semiconducting materials with various lattice constants and band-gap widths. A number of 648 compounds have been calculated with density-functional theory, which allows to obtain general properties and make comparisons between the members of the I-I-VI, I-II-V, I-III-IV, II-II-IV, and II-III-III classes "*in silico*," which means without the need to synthesize a large number of materials. One finds that for many but not all compounds the XYZ configuration is favored. Especially for compounds that consist of main group elements only the XYZ configuration is most stable. In compounds with an XYZ configuration, a particularly stable eight-electron substructure is formed by the $(YZ)^{n-}$ anions. Consequently, most semiconducting half-Heusler compounds have a stable XYZ configuration. Two simple formulas have been derived for approximating the lattice constants of half-Heusler compounds with stable XYZ configuration. The functions depend only on the Slater atomic radii of the components. Geometric considerations provide a parameter-free expression for the equilibrium lattice constants that reasonably approximates the calculated data. A more refined model allows to compare the stiffness of bonds between neighboring sites, showing that the covalent bond between the Y and Z components is the stiffest. The results for the studied compounds can be used to preselect materials for optoelectronic applications. As a practical application, we selected a set of 20 eight-electron half-Heusler compounds that fulfill necessary conditions for replacing CdS as buffer material in CIGSe and CISe thin-film solar cells. For this small number of materials it becomes practical to test the buffer layer properties experimentally.

ACKNOWLEDGMENTS

The author thanks Claudia Felser (Universität Mainz), Reiner Klenk, and David Kieven (Helmholtz-Zentrum Berlin für Materialien und Energie), as well as Johannes Windeln (IBM Mainz) for helpful discussions. Financial support by the BMU (Grant No. 0327665C) is greatfully acknowledged.

*gruhn@uni-mainz.de

[1] E. Zintl, Angew. Chem. **52**, 1 (1939).
[2] C. Kandpal, C. Felser, and R. Seshadri, J. Phys. D **39**, 776 (2006).
[3] H. Nowotny and K. Bachmayer, Monatsch. Chem. **81**, 488 (1950).
[4] R. Juza, K. Langer, and K. V. Benda, Angew. Chem., Int. Ed. Engl. **7**, 360 (1968).
[5] K. Kuriyama, T. Kato, and K. Kawada, Phys. Rev. B **49**, 11452 (1994).
[6] K. Kuriyama, R. Taguchi, K. Kushida, and K. Ushiyama, J. Cryst. Growth **198-199**, 802 (1999).
[7] K. Kuriyama, Y. Yamashita, T. Ishikawa, and K. Kushida, Phys. Rev. B **75**, 233204 (2007).
[8] H. Nowotny and F. Holub, Monatsch. Chem. **91**, 877 (1960).
[9] R. Bacewicz and T. F. Ciszek, Appl. Phys. Lett. **52**, 1150 (1988).
[10] D. M. Wood, A. Zunger, and R. de Groot, Phys. Rev. B **31**, 2570 (1985).
[11] S.-H. Wei and A. Zunger, Phys. Rev. Lett. **56**, 528 (1986).
[12] A. Bouhemadou and R. Khenata, Semicond. Sci. Technol. **23**, 105024 (2008).
[13] A. E. Carlsson, A. Zunger, and D. M. Wood, Phys. Rev. B **32**, 1386 (1985).
[14] L. Spina, Y.-Z. Jia, B. Ducourant, M. Tillard, and C. Belin, Z. Kristallogr. **218**, 740 (2003).
[15] W. Blase, G. Cordier, and R. Kniep, Z. Anorg. Allg. Chem. **619**, 1161 (1993).
[16] W. Bockelmann and H.-U. Schuster, Z. Anorg. Allg. Chem. **410**, 241 (1974).
[17] U. Eberz, W. Seelentag, H. U. Schuster, Z. Naturforsch. B **35**, 1341 (1980).
[18] R. Marazza, D. Rossi, and R. Ferro, J. Less-Common Met. **138**, 189 (1988).
[19] D. Kieven, R. Klenk, S. Naghavi, C. Felser, and T. Gruhn, Phys. Rev. B **81**, 075208 (2010).
[20] G. Jaiganesh, T. M. A. Britto, R. D. Eithiraj, and G. Kalpana, J. Phys.: Condens. Matter **20**, 085220 (2008).
[21] R. Klenk, Thin Solid Films **387**, 135 (2001).
[22] F. Kalarasse and B. Bennecer, J. Phys. Chem. Solids **67**, 1850 (2006).
[23] K. Kuriyama and T. Katoh, Phys. Rev. B **37**, 7140 (1988).
[24] H. Nelson, M. Engelhard, and H. Hochst, J. Electron Spectrosc. Relat. Phenom. **51**, 623 (1990).
[25] K. Kuriyama, T. Katoh, and N. Mineo, J. Cryst. Growth **108**, 37 (1991).
[26] G. K. H. Madsen, P. Blaha, K. Schwarz, E. Sjöstedt, and L. Nördström, Phys. Rev. B **64**, 195134 (2001).
[27] E. Engel and S. H. Vosko, Phys. Rev. A **47**, 2800 (1993).
[28] P. Dufek, P. Blaha, and K. Schwarz Phys. Rev. B **50**, 7279 (1994).
[29] K. Kuriyama and K. Kushida, J. Appl. Phys. **87**, 3168 (2000).
[30] K. Kuriyama, K. Nagasawa, and K. Kushida, J. Cryst. Growth **237-239**, 2019 (2002).
[31] K. Kuriyama and K. Kushida, Solid State Commun. **112**, 429 (1999).
[32] K. Kuriyama, K. Kushida, and R. Taguchi, Solid State Commun. **108**, 429 (1998).
[33] K. Kuriyama, T. Kato, and T. Tanaka, Phys. Rev. B **49**, 4511 (1994).
[34] J. Slater, J. Chem. Phys. **41**, 3199 (1964).
[35] The efficiency record of 20.1% has been announced by the "Zentrum für Sonnenenergie und Wasserstoff-Forschung Baden-Württemberg (ZSW)" in a press release, May 2010.
[36] D. Hariskos, S. Spiering, and M. Powalla, Thin Solid Films **480-481**, 99 (2005).
[37] M. Bär, J. Reichardt, I. Sieber, A. Grimm, I. Kötschau, I. Lauermann, S. Sokoll, T. P. Niesen, M. C. Lux-Steiner, and C.-H. Fischer, Prog. Photovoltaics **15**, 187 (2007).
[38] B. T. Ahn, L. Larina, K. H. Kim, and S. J. Ahn, Pure Appl. Chem. **80**, 2091 (2008).
[39] S. Schorr and G. Geandier, Cryst. Res. Technol. **41**, 450 (2006).
[40] K. Jones, J. Cryst. Growth **47**, 235 (1979).
[41] N. Razik, J. Mater. Sci. Lett. **6**, 1443 (1987).
[42] Y. Kanemitsu, T. Nagai, T. Kushida, S. Nakamura, Y. Yamada, and T. Taguchi, Appl. Phys. Lett. **80**, 267 (2002).
[43] H. Goto, Y. Hashimoto, and K. Ito, Thin Solid Films **451-452**, 552 (2004).
[44] D. Kieven, A. Grimm, A. Beleanu, C. G. F. Blum, J. Schmidt, T. Rissom, I. Lauermann, T. Gruhn, C. Felser, and R. Klenk, Thin Solid Films(to be published).